Comprehensive examination of dopants and defects in $BaTiO_3$ from first principles

V. Sharma,[1] G. Pilania,[1] G. A. Rossetti, Jr.,[1] K. Slenes,[2] and R. Ramprasad[1,*]

[1]*Materials Science and Engineering, Institute of Materials Science, University of Connecticut, Storrs, Connecticut 06269, USA*

[2]*TPL, Inc., 3921 Academy Parkway North, NE, Albuquerque, New Mexico 87109, USA*

(Received 3 March 2013; published 30 April 2013)

An extensive assessment of the physicochemical factors that control the behavior of dopant-related defects in $BaTiO_3$ has been performed using high-throughput first-principles computations. Dopants spanning the Periodic Table—44 in total—including K-As, Rb-Sb, and Cs-Bi were considered, and have allowed us to reveal previously unknown correlations, chemical trends, and the interplay between stability, chemistry, and electrical activity. We quantitatively show that the most important factor that determines dopant stability in $BaTiO_3$ is the dopant ionic size (followed by its oxidation state). Moreover, we are also able to identify definitively dopants that are O vacancy formers and suppressors, and those that would lead to *p*-type versus *n*-type conduction. Our results are in agreement with available experimental data (with no violations thus far), and point to an attractive computational route to dopant selection in $BaTiO_3$ as well as in other materials.

DOI: 10.1103/PhysRevB.87.134109 PACS number(s): 61.72.S−, 77.84.Bw, 71.15.Mb

I. INTRODUCTION

One pathway for achieving materials with new or improved properties is imaginative chemical modification. This has been particularly exploited in perovskites with the chemical formula ABO_3 (with A and B being cations)—materials that have found solutions in diverse technological applications in fields ranging from electronics to sensors to catalysis.[1–6] Owing to the intrinsic capability of the perovskite structure to host ions of various sizes across the Periodic Table, a wide range of dopants can be, and have been, successfully accommodated in the ABO_3 structures. In fact, the chemical doping of ABO_3 compounds is essential in many applications, e.g., to tune the band gap of the host material,[7] to enhance or suppress oxygen ion formation and conductivity,[8,9] to manipulate and control the electrical and electroactive behavior,[10,11] to tune physical properties such as the Curie temperature and domain switching,[12,13] and more recently, to optimize the electrochemical or catalytic activity of the host material.[14,15]

Within the class of ABO_3 perovskite-type materials, $BaTiO_3$ (BTO) is perhaps the most widely used[7–23] and studied[6,24–26] multifunctional ceramic material. The extensive body of past experimental[27–33] and theoretical[34–36] studies of dopants in BTO has lead to enormous insights, which continue to grow. Still, the underlying strategies that have been adopted in most past studies have largely been Edisonian—typically, such approaches are motivated by specific hypotheses, encompass comparatively limited ranges of dopant type and concentration, and involve particular experimental conditions and/or differing levels of theory. As a result, several of the critical questions pertaining to general physicochemical trends for dopants across the Periodic Table have remained mostly unanswered for a long time.[30–37] These include: (i) How thermodynamically favorable would it be to incorporate a given dopant in BTO? (ii) Which cation site (i.e., Ba or Ti) would the dopant prefer to occupy, and what are the fundamental factors that govern this tendency? (iii) Which dopants enhance or suppress the formation of O vacancies (O_{vac}), and why? (iv) Can the electrical nature of a dopant (i.e., whether it is *p*-type or *n*-type) be related to factors such as the nominal oxidation state or the tendency for O_{vac} formation? Answering such questions satisfactorily can provide a fundamental basis for Hume-Rothery-like rules[38] for this particular class of materials, and enable efficacious dopant selection to meet a given need.

Here, we seek to address the above questions using high-throughput density functional theory (DFT) calculations. To explore the underlying physicochemical trends pertaining to dopants across the Periodic Table, we have considered the 3*d*, 4*d*, and 5*d* transition metals along with the neighboring IA through VA Group elements in our analysis. This includes the elements K-As, Rb-Sb, and Cs-Bi. To understand the site-dependent behavior, dopants at both Ba and Ti sites were considered. The regularities governing the dopant properties (e.g., the energy to form a dopant with and without an adjacent O_{vac}, structural and electronic structure distortions, etc.) were investigated in an attempt to determine the most important crystallochemical factors that determine the interplay between stability, chemistry and electrical activity.

II. METHODS

Our systematic first-principles assessment of dopant chemistry in BTO is performed using a $2 \times 2 \times 2$ supercell containing a total of eight BTO formula units (i.e., containing 40 atoms). Spin-polarized calculations are performed using the projector augmented plane wave basis functions as embodied in the Vienna *ab initio* simulation package (VASP).[39–41] The exchange correlation interaction is treated within the generalized gradient approximation (GGA) using the Perdew-Burke-Ernzerhoff (PBE) functional,[42] as GGA is reasonably accurate in calculating energy differences between compounds with delocalized states.[43] The relaxation of atomic positions and optimization of lattice parameters are performed by the conjugate gradient method. The atomic positions are relaxed until the maximum component of the force on each atom is smaller than 0.02 eV/Å. A Monkhorst-Pack *k*-point mesh[44] of $8 \times 8 \times 8$ is employed to produce converged results within 0.1 meV per formula unit. The density of states (DOS) is calculated by the linear tetrahedron method with Blöchl corrections.[45]

Dopants across the Periodic Table were then introduced either in the Ba or the Ti site of our 40-atom BTO supercell,

thereby resulting in a dopant concentration of 12.5%. The dopant atoms explored consisted of K-As, Rb-Sb, and Cs-Bi, thus totalling 44 cases for each site (not including Ba and Ti, the host atoms). Interstitial doping was not studied owing to the large size of the dopants considered here. To evaluate the energetics of dopant formation, we define the 0 K dopant formation energy, E_f^D, as

$$E_f^D = E_{\mathrm{BTO}}^D - E_{\mathrm{BTO}}^H - (\mu^D - \mu^H), \quad (1)$$

where E_{BTO}^D and E_{BTO}^H are, respectively, the DFT energies of the doped and undoped BTO supercells, and μ^D and μ^H are, respectively, the elemental chemical potentials of the dopant and the replaced host atoms. In addition, a separate set of calculations involving an O_{vac} adjacent to the dopant atom was also performed, in order to probe the tendency for dopant-induced O_{vac} formation. The combined formation energy of a dopant *and* an O_{vac} ($E_f^{D\text{-}O_{vac}}$) was determined as

$$E_f^{D\text{-}O_{vac}} = E_{\mathrm{BTO}}^{D\text{-}O_{vac}} - E_{\mathrm{BTO}}^H - \left(\mu^D - \mu^H - \tfrac{1}{2}\mu_{O_2}\right), \quad (2)$$

where $E_{\mathrm{BTO}}^{D\text{-}O_{vac}}$ is the DFT total energy of the supercell containing a dopant and an adjacent O_{vac}, and μ_{O_2}, the oxygen chemical potential, is taken to be the DFT energy of an isolated O_2 molecule in the gas phase. We also note that the O_{vac} formation energy, $E_f^{O_{vac}}$, in any given case of dopant (and site) is simply given by the difference of the above two formation energies, i.e.,

$$E_f^{O_{vac}} = E_f^{D\text{-}O_{vac}} - E_f^D. \quad (3)$$

The formation energies defined above depend on the particular choice of the atomic chemical potentials. In the present study, the chemical potential of either the host or the dopant atoms, μ^M, is defined using the total energies of the most stable oxides of the respective dopant and host atoms as

$$\mu^M = \frac{1}{y}\left(E_{M_yO_x} - \frac{x}{2}\mu_{O_2}\right), \quad (4)$$

where $E_{M_yO_x}$ is the DFT energy of the most stable oxide M_yO_x, where M represents either the host or the dopant atom, and x and y represent the stoichiometry of the oxide. Furthermore, the formation energy of the dopant and host simple oxide may be defined as

$$E_f^{M_yO_x} = \frac{1}{y}\left(E_{M_yO_x} - \frac{x}{2}\mu_{O_2} - yE_{\mathrm{Bulk}}\right) = \mu^M - E_{\mathrm{Bulk}}, \quad (5)$$

where E_{Bulk} is the DFT energy of the most stable bulk elemental solid formed from the dopant and host atoms, respectively.

Prior to investigating dopants in BTO, we first desire to confirm the level of accuracy that may be expected at the level of theory used here (namely, the semilocal PBE exchange-correlation functional). One way this can be done is to compare the simple oxide formation energies computed using Eq. (5) with the corresponding experimental values.[46] Such a comparison, portrayed in Fig. 1, immediately shows that our DFT-computed results are uniformly shifted by 0.77 eV. This is a well-known deficiency, which can in turn be traced to the overbinding of the O_2 molecule within the GGA methodology.[47–50] Therefore, in order to recover the experimental dopant formation energetics, the DFT O_2 molecular energy has been destabilized by 0.77 eV. We note that this correction is consistent with the previously suggested value of 0.79 eV.[49,50]

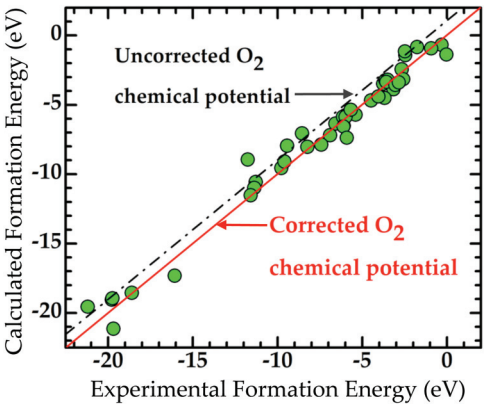

FIG. 1. (Color online) Computed and experimental (Ref. 46) formation energies of the 45 stable simple oxides (of K-As, Rb-Sb, and Cs-Bi), relevant to the present study. The solid line fit corresponds to the −0.77 eV energy correction required to account for the GGA overbinding of the O_2 molecule. The dashed line corresponds to the fit obtained when the formation energies were computed using the uncorrected oxygen chemical potential.

III. RESULTS AND DISCUSSIONS

A. Structural details

The calculated lattice parameter (4.071 Å) and the rhombohedral angle (89.74°) for pure BTO, are in good agreement with the corresponding experimental values[51] (4.004 Å and 89.8°, respectively) and past theoretical results[52] (cf. Ref. 50 and references therein). Introduction of the dopants at the Ba or the Ti sites preserved the rhombohedral symmetry of the overall supercell at the dopant concentration considered. For instance, as shown in Fig. 2(a) for just the Ti-site doping, the relevant rhombohedral angle varies between 89.60° to 89.95°. The lattice parameter of the doped systems shows variations that may be understood based on the ionic radius of the corresponding dopant atoms. Figure 2(b) portrays the variation of the lattice constant (defined with respect to undoped BTO) for the Ti-site doping, and Fig. 2(c) displays the Shannon's ionic radius[53] of all systems considered, corresponding to the oxidation state and coordination environment of the cations in their most stable oxides at 0 K.[46] It is clear that the gyrations displayed by the lattice constant can be correlated to the ionic radius variations across the Periodic Table. Figure 2(b) also shows available experimental lattice parameter values for BTO doped with Co,[27] Cr,[27] Fe,[27] Mn,[32] Nb[54] at about the same dopant concentrations as considered here. It can be seen that our results are in close agreement with experiments.

B. Dopant formation energy

The calculated dopant formation energies for both the Ba and the Ti site substitutions are depicted in Figs. 3(a)–3(c) and help us to answer the question related to site preference of the dopants. It can be seen immediately that the vast majority of the dopants prefer to replace Ti. The sole exceptions (i.e., the

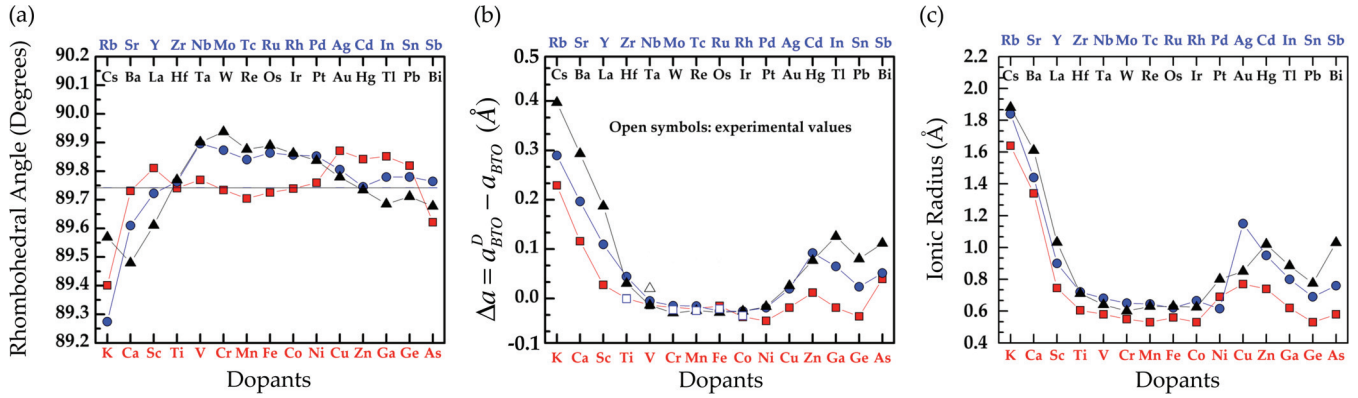

FIG. 2. (Color online) (a) Variation of the rhombohedral angle as a function of dopant (at the Ti site). The horizontal line indicates the value corresponding to undoped BTO. (b) Variation of lattice parameter as a function of dopant (at the Ti site) along with available experimental results. (c) The effective Shannon's ionic radius of dopants. A comparison of (b) and (c) indicates a close correlation between the dopant ionic radius and the lattice constant of doped BTO.

dopants that favor the Ba site) are the Group IA elements K, Rb, Cs, the Group IIA elements Ca, Sr, Ba, and the transition metal elements Cd and Hg. These findings are consistent with past experimental work, which show that K,[55] Ca,[56] and Sr[30] prefer the Ba site, and transition metal elements from the 3*d* series (Cr, Mn, Fe, Co, Ni Cu, Zn),[27–32] the 4*d* series (Zr, Nb, Mo, Rh, Cd),[54,57–62] and the 5*d* series (Hf, Ta, Re)[62–64] along with Group IIIA elements (Ga, In)[17] prefer the Ti site. Interestingly, a crossover between the preference for Ba site to Ti site can be seen between Ca and Sc (3*d* series), Sr and Y (4*d* series), and Ba and La (5*d* series). Likewise, crossovers can also be seen in the late transition metal regime as well, e.g., between Ag and Cd (4*d* series) and between Hg and Tl (5*d* series). Indeed, interestingly, experimental work shows that Ca,[21,65] Y,[66] Cd,[59] and La[67,68] can occupy the Ba or Ti sites in BTO, consistent with our predicted crossover trends. Figure 3 also shows that a large preference for Ti substitutions over Ba substitutions (as indicated by the difference in the dopant formation energies) is displayed by the early transition metal elements, and this preference diminishes for the late transition metal elements.

The dopant formation energies portrayed in Fig. 3 clearly display interesting trends across the Periodic Table. In order to understand the dominant factors that control the observed trends, we attempted to relate several properties of the dopant atoms to the computed formation energy. These properties included the ionic size, oxidation state, electronegativity, polarizability, ionization potential, and electron affinity. Of all these properties, the ionic radius and the oxidation state of the dopant atom appear to correlate best, and are able to explain the trends in the computed dopant formation energy. Here, we use Shannon's ionic radius and the oxidation state value corresponding to the dopant atom in its most favored oxide. The correlations are depicted in Fig. 4.

Conventional wisdom dictates that in order to preserve the charge neutrality of the system, substitution of a dopant with the same oxidation number as the host is thermodynamically more stable. This is also consistent with our findings, where the formation energy correlates well with the dopant oxidation state. In Fig. 4(a), we have plotted the dopant formation energies as a function of variation in oxidation state of dopant with respect to the host atom. As can be seen, dopants with nominal oxidation states identical or closest to the host atom they replace (i.e., 2 in the case of Ba, and 4 in the case of Ti) generally have low dopant formation energy. We note though that there is a significant variation in the dopant formation

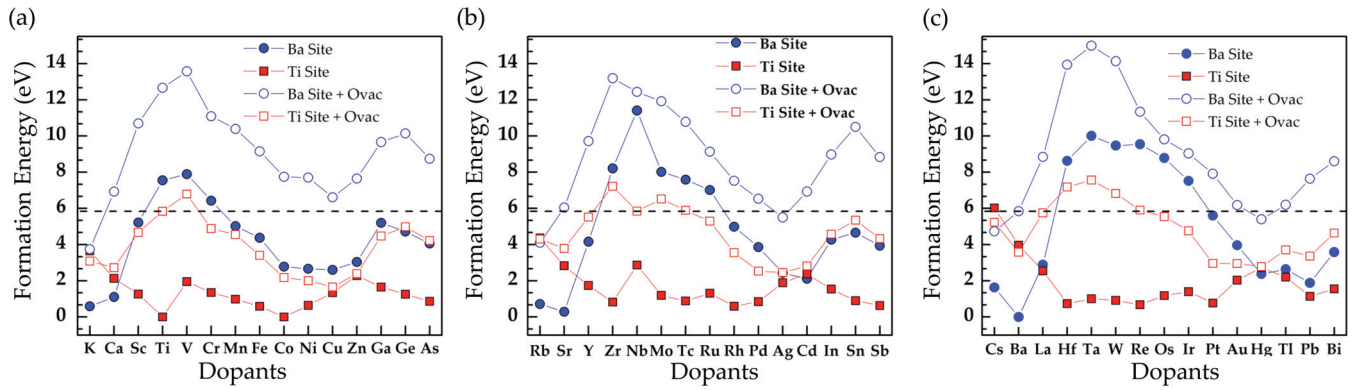

FIG. 3. (Color online) Calculated formation energies for introducing a dopant (at the Ba or Ti site), and a dopant in the presence of adjacent O_{vac} in BTO, for dopants in the (a) 3*d*, (b) 4*d*, and (c) 5*d* series along with their neighboring Group IA to VA elements of the Periodic Table. Circle and square correspond to dopant at Ba and Ti site, respectively, while open (filled) symbols represent the dopant in presence (absence) of O_{vac}.

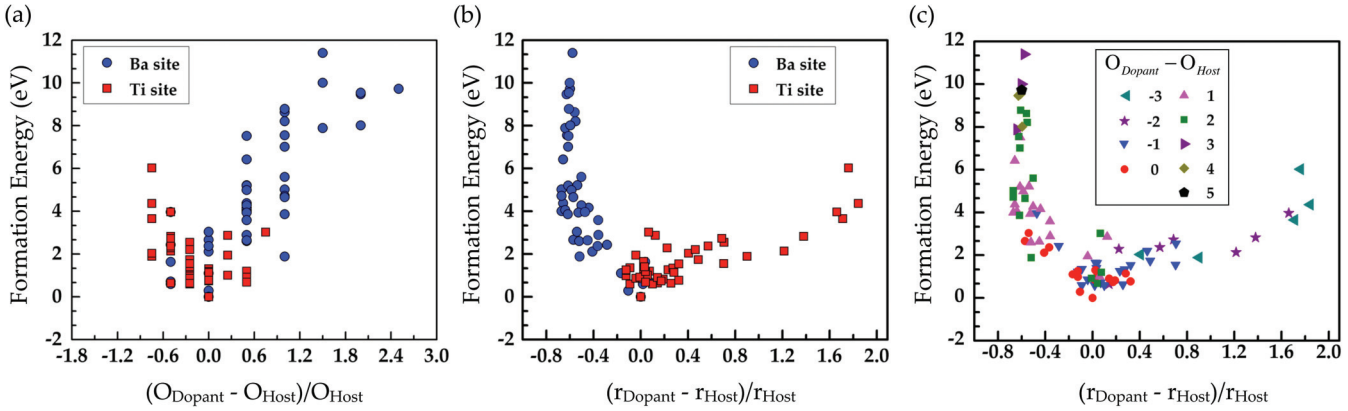

FIG. 4. (Color online) Calculated dopant formation energies as a function of variation in (a) the oxidation state, and (b) the ionic radius of the dopants relative to the host atom. (c) Same as (b), but with the dopants distinguished by their oxidation states (relative to that of the host atom the replace) using different symbols.

energy for dopants with the same oxidation state [Fig. 4(a)]. These large variations may be explained by considering the size factor, i.e., the ionic radius of the dopant relative to that of the host atom. It can be seen [from Fig. 4(b)] that dopants with ionic radius closest to that of the host atom they replace lead to the lowest dopant formation energy, and dopants whose ionic size deviates significantly from that of the host atom display the opposite behavior. It is noted that similar to Fig. 4(a), Fig. 4(b) also displays a near-parabolic trend, albeit with a clear asymmetry and significantly less variation than in Fig. 4(a), indicating that the size factor is even more important than the oxidation state. Other properties (electronegativity, electron affinity, ionization potential, and polarizability) were also considered in an attempt to draw similar correlations, but these properties did not lead to a clear understanding of the dopant formation energy trends.

The above perceptions are even more clearly captured in Fig. 4(c), in which the dopant formation energy is plotted against the relative ionic radius of dopant for both Ba and Ti site doping along with the relative oxidation states appropriately indicated using different symbols. Based on the present analysis, we conclude that the most important factor that determines the dopant formation energy is the difference in the ionic radii of the dopant and the host atom, and the second most important factor is the difference in the oxidation states (with all other factors being of lower importance).

C. O_{vac} formation energy

The presence of O_{vac} substantially affects the behavior and performance of BTO in ferroelectric memories, dielectric capacitors, and energy conversion devices.[69–73] Furthermore, O_{vac} are known to have significant influence in oxygen transport.[69] For example, in solid oxide fuel cells, O_{vac} enable transport of O^{-2} ions through the oxide electrolyte membrane over a range of temperatures. Recently, it has been observed that ferroelectric perovskites modified by M^{+2}-O_{vac} substitution provide a promising route for designing highly polar semiconducting oxides suitable for photovoltaic applications.[70,71] Another interesting possibility of utilizing O_{vac} for technological application is deliberate control of O_{vac} concentration.[72,73] Therefore, a detailed knowledge of the stability and the nature of the formation of O_{vac} in BTO is essential from the point of view of designing novel materials by tailoring its properties for a specific technical application.

Our results for the dopant formation energies in the presence of an adjacent O_{vac} are summarized in Figs. 3(a)–3(c). The open symbols represent the formation energy to simultaneously create a dopant *and* an adjacent O_{vac}, $E_f^{D\text{-}O_{vac}}$, as defined in Eq. (2). The O vacancy formation energy, $E_f^{O_{vac}}$ is the difference in energy represented by the open and filled symbols [as defined in Eq. (3)]. We note that while the latter quantity (namely, $E_f^{O_{vac}}$) is widely discussed, it is the former that is relevant in fair assessments of favorable situations spanning different dopants. The energy associated with the creation of a neutral O_{vac} in pure BTO is 5.84 eV, shown as a reference horizontal dashed line in each of the three panels in Fig. 3. The results of Fig. 3 may also be used to identify dopants that particularly favor or disfavor the formation of O_{vac} with respect to the undoped system.

It can be immediately concluded from Fig. 3 that O_{vac} formation in presence of a dopant ($E_f^{D\text{-}O_{vac}}$) is favored when the dopant is situated at the Ti site rather than at the Ba site. This behavior can be understood in terms of a charge compensation mechanism, which dictates that the lowest O_{vac} formation energy should be achieved in the presence of dopants favoring a $+2$ nominal oxidation state at the Ti site. Furthermore, following the above rationale we would expect O_{vac} formation to be energetically costlier for the Ba site doping as compared to that for the Ti site. We find that our calculated oxygen vacancy formation energies, reported in Figs. 3(a)–3(c), are indeed in line with these notions and show a good agreement with reported experimental observations.[28]

We note that the transition metals, including Cr-Zn (3*d* series), Rh-Cd (4*d* series), and Pt-Hg (5*d* series) are particularly good O_{vac} formers, with the increased tendency for O_{vac} formation shifting to later in the series as we go from 3*d* to 4*d* to 5*d* elements. On the contrary, dopants such as V, Zr, Mo, Hf, Ta, and W are O_{vac} suppressors as $E_f^{D\text{-}O_{vac}}$ corresponding to these cases are above the dashed line in Fig. 3. These findings are consistent with available experimental data; it is known that Mn, Fe, Co, and Ni lead to a high concentration of O_{vac},[74] whereas Nb,[57,58] La,[75] Mo,[61] and Ta,[63] favor the formation of

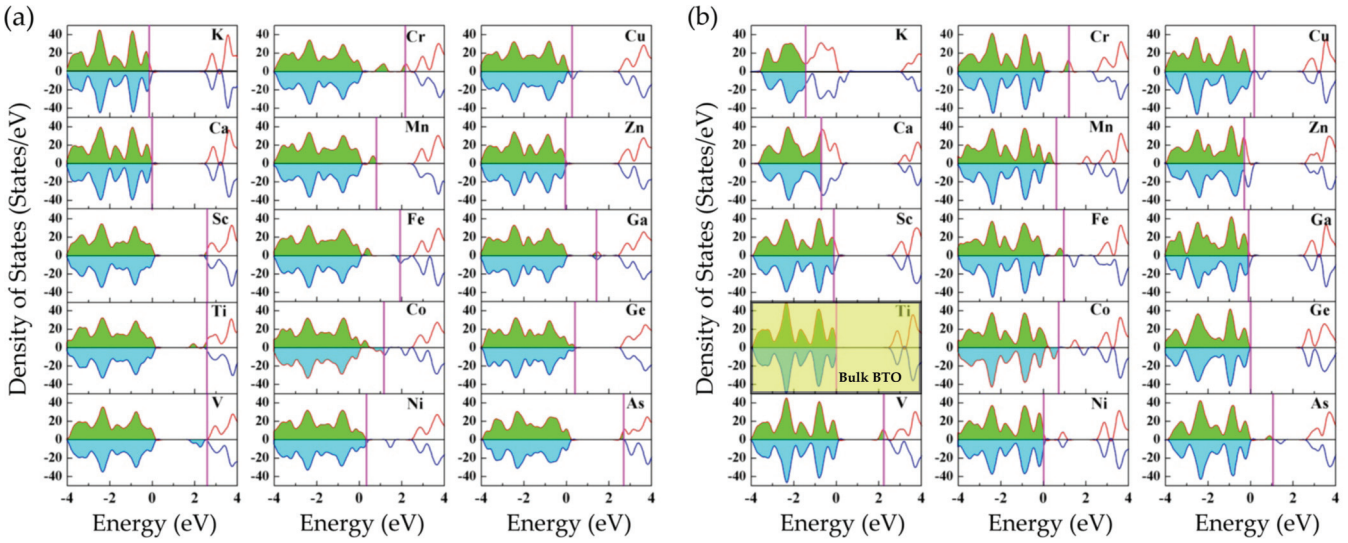

FIG. 5. (Color online) Calculated total density of states of BTO doped at the (a) Ba site, and at the (b) Ti site, with the 3*d* transition and neighboring Group IA to VA elements. The highlighted panel shows the DOS of pure BTO. The vertical line corresponds to the Fermi level, obtained by alignment of electrostatic potentials of the defect supercell and pure BTO.

cation vacancies (and hence display a tendency to suppress O_{vac} formation).

In order to identify the most relevant crystallochemical factors of a dopant that govern the O_{vac} formation in presence of the dopant, we considered $E_f^{O_{vac}}$ as a function of the difference of the ionic radii and oxidation states of the dopant and the host atoms (analogous to our analysis of E_f^D). We observed that dopants that are larger than the host atoms (by about 30%) or those with lower oxidation state than the host atom (by 2 or less) lead to low $E_f^{O_{vac}}$. Thus the ideal dopant that will lead to copious O_{vac} are Co, Ni, Cu, Zn, Pd, Ag, Cd, Pt, Au, and Hg, which have a lower oxidation states ($\leqslant$2), while V, Nb, Mo, Tc, Ta, W, and Re are found to be O_{vac} suppressors.

D. Electronic structure

Since the electrical nature (i.e., the *n*-type or *p*-type behavior) exhibited by a dopant after incorporation in BTO is crucial for a range of applications,[13,29–33,56,76,77] we consider the electronic structure of pure and doped BTO to predict the conductivity behavior of all the dopants studied here. We find that our calculated band gap (2.6 eV), electronic band structure and the density of states (DOS) for pure BTO are in close agreement with prior results performed at a similar level of theory.[52,78] Given that the semilocal electronic exchange-correlation functional adopted here is known to underestimate the band gap of insulators (and places an uncertainty in the energetic position of dopant-derived defect levels), we make the caveat that the following conclusions should be viewed as qualitative. While it may be desirable to perform more sophisticated computations (e.g., using hybrid functionals) to ascertain the validity of the emerging notions pertaining to the electronic structure, these have not been attempted in the present work. The DOS plots for both the Ba and Ti site doping situations for the 3*d* series dopants and neighboring Group IA to VA elements are shown in Figs. 5(a)–5(b). The DOS plots for the dopants belonging to the 4*d* and 5*d* series as well as the Group IA to VA elements display similar qualitative behavior. The Fermi level, indicated by a vertical line in each of the panels in Fig. 5, was determined by realigning the average electrostatic potential of the defect containing supercell (taken at a sufficient distance away from the defect so that a bulklike behavior is recovered) to that of the defect-free bulk BTO.

As a general trend, Fig. 5 clearly shows that the dopants exhibiting a higher (lower) oxidation state as compared to the atom they substitute show an *n*-type (*p*-type) behavior. However, it can also be seen from Fig. 5 that certain dopants may adjust their nominal oxidation states according to the local coordination environment upon incorporation in the host. For instance, when substituted at the Ba site, the Mn and Ge atoms tend to adopt a $+2$ oxidation state, while at the Ti site these dopants prefer to stay in a $+4$ oxidation state. A similar behavior is also observed for the Tc, Re, Sn, and Pb dopants. The above predictions may also provide a justification for the experimental observations that the above-mentioned isovalent impurities decrease leakage currents in important device applications.[76]

The collective information regarding the dopants' site preferences, electrical nature as well as the stable oxidation state on that site along with the calculated formation energies (both in the presence and absence of a neighboring O_{vac}) is captured in Figs. 6(a)–6(c). Interestingly, it can be seen from the plot that the tendency of a dopant to favor or disfavor formation of an O_{vac} in BTO is correlated with its electrical nature. In line with the electron counting notions, *p*-type (*n*-type) dopants tend to promote (suppress) the formation of oxygen vacancies in BTO. Figure 6 also reveals that most of the TMs as well as the dopants from Groups IA, IIIA, and VA are of *p*-type nature and favor the Ti site substitution. On the other hand, only a handful of dopants, that can exhibit a higher oxidation state than that of the the Ti atom, (for instance, V^{5+}, Nb^{5+}, Mo^{6+}, Tc^{7+}, Ta^{5+}, W^{6+}, and Re^{6+}) show an *n*-type behavior. These findings are also found to be consistent with available experimental results (Nb,[57,58,63] Mo,[61] and Ta[63]).

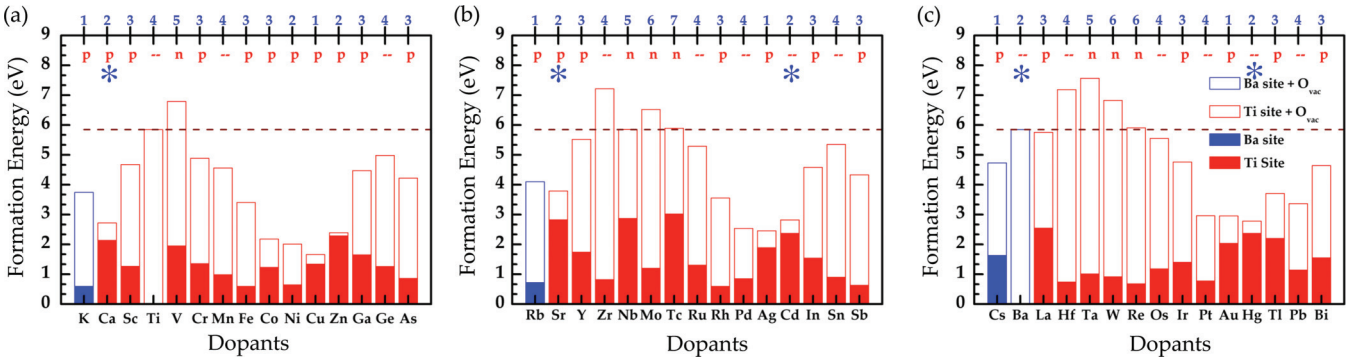

FIG. 6. (Color online) Calculated dopant formation energies in the presence (open) and the absence (solid) of an O_{vac}. Blue and red colors correspond to the dopant at the Ba and Ti sites, respectively. An asterisk (*) indicates cases in which the Ba site is favored in the absence an O_{vac}, but the Ti site is favored in the presence of an O_{vac}. The nominal oxidation state and the electrical nature of a dopant are depicted on the top horizontal axis.

IV. SUMMARY

In this contribution, we have presented a comprehensive and systematic first-principles investigation (at a single consistent level of theory) of a large variety of dopants—44 in all, including K-As, Rb-Sb and Cs-Bi—incorporated at the Ba and Ti sites of $BaTiO_3$ (BTO). Consideration of this large number of elements from across the Periodic Table has allowed us to effectively confirm past chemical intuition as well as to properly capture and recognize physicochemical trends. Below, we list the notions and general guidelines that have emerged from this study:

(1) The dominant factor that controls the stability and the location of a dopant in BTO appears to be the ionic size of the dopant. The closer the dopant size is to that of the host atom, the smaller is its formation energy. The residual scatter in the formation energy data (after accounting for the dependence on the ionic size) may be explained by the nominal oxidation state of the dopant with respect to that of the host atom it replaces.

(2) For the above-mentioned reasons, the alkali and alkaline earth elements prefer to be situated at the Ba site, while the vast majority of the transition metal dopants favor the Ti site. Ca, Sc, Sr, Y, Ba, La, Ag, Cd, Hg, and Tl appear to prefer the Ba and Ti sites roughly equally.

(3) At the Ti site, the tendency for O vacancy (O_{vac}) formation is enhanced by the dopants with an ionic radius larger than that of the Ti by about 30%, and a nominal oxidation state of 2 or less. Therefore, Co, Ni, Cu, Zn, Pd, Ag, Cd, Pt, Au, Hg at the Ti site would favor O_{vac} formation more than in in undoped $BaTiO_3$, while V, Nb, Mo, Tc, Ta, W, and Re are predicted to be O_{vac} suppressors.

(4) In contrast to the Ti site doping, control of O_{vac} concentration through Ba site doping appears relatively less tunable. While most of the dopants remain O_{vac} suppressors, Group IA dopants (i.e., K, Rb, and Cs) alone promote O_{vac} formation at this site.

(5) As dictated by electron counting notions, the tendency of a dopant to promote or suppress O_{vac} formation in BTO is correlated with its electrical nature. In general, *p*-type (*n*-type) dopants lead to a favorable (unfavorable) situation for the formation of oxygen vacancies in BTO.

It is worth noting that all of our conclusions are in agreement with available experimental data (with no violations thus far), attesting to the trustworthiness one may attach to such chemical space explorations. Given that experimental analysis and screening of dopants in oxides is a time consuming and costly enterprise, modern first-principles computational approaches may be viewed as an alternative and complementary route to dopant selection in important technical materials.

ACKNOWLEDGMENTS

This material is based upon work supported by an Air Force STTR subcontract from TPL, Inc. Partial computational support through a National Science Foundation Teragrid allocation is also gratefully acknowledged. The authors also thank Clive Bealing for a critical reading of the manuscript.

*rampi@uconn.edu

[1] G. H. Haertling, J. Am. Ceram. Soc. **82**, 797 (1999).
[2] J. M. Wilson, Am. Ceram. Soc. Bull. **74**, 106 (1995).
[3] J. S. Capurso, A. A. Bologna, and W. A. Schulze, J. Am. Ceram. Soc. **78**, 2476 (1995).
[4] A. Rae, M. Chu, and V. Ganine, in *Ceramic Transactions, Dielectric Ceramic Materials*, edited by K. M. Nair and A. S. Bhalla (The American Ceramic Society, Westerville, OH, 1999), Vol. 100, pp. 1–12.
[5] X. Ren, Nature Mater. **3**, 91 (2004).
[6] A. S. Bhalla, R. Guo, and R. Roy, Mater. Res. Innovations **4**, 3 (2000).
[7] S. Upadhyay, J. Shrivastava, A. Solanki, S. Choudhary, V. Sharma, P. Kumar, N. Singh, V. R. Satsangi, R. Shrivastav, U. V. Waghmare, and S. Dass, J. Phys. Chem. C **115**, 24373 (2011).
[8] C. Metzmacher and K. Albertsen, J. Am. Ceram. Soc. **84**, 821 (2001).
[9] A. Honda, S. Higai, Y. Motoyoshi, N. Wada, and H. Takagi, Jpn. J. Appl. Phys. **50**, 09NE01 (2011).
[10] A. D. Caviglia, S. Gariglio, N. Reyren, D. Jaccard, D. Schneider, M. Gabay, S. Thiel, G. Hammerl, J. Mannhart, and J.-M. Triscone, Nature (London) **456**, 624 (2008).

[11]H. Ohta, S. Kim, Y. Mune, T. Mizoguchi, K. Nomura, S. Ohta, T. Nomura, Y. Nakanishi, Y. Ikuhara, M. Hirano, H. Hosono, and K. Koumoto, Nature Mater. **6**, 129 (2007).
[12]J.-H. Jeon, J. Eur. Ceram. Soc. **24**, 1045 (2004).
[13]H.-J. Hagemann and D. Hennings, J. Am. Ceram. Soc. **64**, 590 (1981).
[14]J. Suntivich, K. J. May, H. A. Gasteiger, J. B. Goodenough, and Y. Shao-Horn, Science **334**, 1383 (2011).
[15]J. Suntivich, H. A. Gasteiger, N. Yabuuchi, H. Nakanishi, J. B. Goodenough, and Y. Shao-Horn, Nature Chem. **3**, 546 (2011).
[16]J. K. Lee, J. S. Park, K. S. Hong, K. H. Ko, and B. C. Lee, J. Am. Ceram. Soc. **85**, 1173 (2002).
[17]L. A. Xue, Y. Chen, and R. J. Brook, Mater. Sci. Eng. B **1**, 193 (1988).
[18]Z.-G. Zhou, Z.-L. Tang, and Z.-T. Zhang, Sensors and Actuators B **93**, 356 (2003).
[19]D. Cao, M. Q. Cai, Y. Zheng, and W. Y. Hua, Phys. Chem. Chem. Phys. **11**, 10934 (2009).
[20]N. V. Dang, T. D. Thanh, L. V. Hong, V. D. Lam, and T.-L. Phan, J. Appl. Phys. **110**, 043914 (2011).
[21]S.-H. Yoon, S.-H. Kang, S.-H. Kwon, and K.-H. Hur, J. Mater. Res. **25**, 2135 (2011).
[22]G. J. Reynolds, M. Kratzer, M. Dubs, H. Felzer, and R. Mamazza, Materials **5**, 575 (2012).
[23]Z. Yan, Y. Guo, G. Zhang, and J.-M. Liu, Adv. Mater. **23**, 1351 (2011).
[24]A. M. Stoneham and L.W. Smith, J. Phys.: Condens. Matter **3**, 225 (1993).
[25]M. A. Pena and J. L. G. Fierro, Chem. Rev. **101**, 1981 (2001).
[26]P. K. Panda, J. Mater. Sci. **44**, 5049 (2009).
[27]H. Liu, B. Cao, and C. O'Connor, J. Appl. Phys. **109**, 07B516 (2011).
[28]M. T. Biscaglia, V. Buscaglia, M. Viviani, P. Nanni, and M. Hanuskova, J. Eur. Ceram. Soc. **20**, 1997 (2000).
[29]N.-H. Chan and D. M. Smyth, J. Electrochem. Soc. **123**, 1584 (1976).
[30]H. Ihrig, J. Am. Ceram. Soc. **64**, 617 (1981).
[31]H. Ihrig, J. Phys. C: Solid State Phys. **11**, 819 (1978).
[32]J. R. Sambrano, E. Orhan, M. F. C. Gurgel, A. B. Campos, M. S. Goes, C. O. P. Santos, J. A. Varela, and E. Longo, Chem. Phys. Lett. **402**, 491 (2005).
[33]D. M. Smyth, J. Electroceram. **9**, 179 (2002).
[34]H. Nakayama and Katayama-Yoshida, Jpn. J. Appl. Phys., Part 2 **40**, L1355 (2001).
[35]G. V. Lewis and C. R. A. Catlow, J. Phys. Chem. Solids **47**, 89 (1986).
[36]M. T. Buscaglia, V. Buscaglia, M. Viviani, and P. Nanni, J. Am. Ceram. Soc. **84**, 376 (2001).
[37]M. J. Akhtar, Z.-U.-N. Akhtar, R. A. Jackson, and C. R. A. Catlow, J. Am. Ceram. Soc. **78**, 421 (1995).
[38]W. Hume-Rothery and G. V. Raynor, Proc. R. Soc. A **174**, 471 (1940).
[39]G. Kresse and J. Hafner, Phys. Rev. B **49**, 14251 (1994).
[40]G. Kresse and J. Furthmuller, J. Comput. Mater. Sci. **6**, 15 (1996).
[41]G. Kresse and J. Furthmuller, Phys. Rev. B **54**, 11169 (1996).
[42]J. P. Perdew, K. Burke, and M. Ernzerhof, Phys. Rev. Lett. **77**, 3865 (1996).
[43]S. Curtarolo, D. Morgan, and G. Ceder, Calphad **29**, 163 (2005).
[44]H. J. Monkhorst and J. D. Pack, Phys. Rev. B **13**, 5188 (1976).
[45]P. E. Blöchl, O. Jepsen, and O. K. Andersen, Phys. Rev. B **49**, 16223 (1994).
[46]http://www.materialsproject.org/
[47]C. Franchini, R. Podloucky, J. Paier, M. Marsman, and G. Kresse, Phys. Rev. B **75**, 195128 (2007).
[48]B. Hammer, L. B. Hansen, and J. K. Nørskov, Phys. Rev. B **59**, 7413 (1999).
[49]L. Wang, T. Maxisch, and G. Ceder, Phys. Rev. B **73**, 195107 (2006).
[50]A. Jain, G. Hautier, C. J. Moore, S. P. Ong, C. C. Fischer, T. Mueller, K. A. Persson, and G. Ceder, Comput. Mater. Sci. **50**, 2295 (2011).
[51]G. H. Kwei, A. C. Lawson, and S. J. L. Billinge, J. Phys. Chem. **97**, 2368 (1993).
[52]R. A. Evarestov and A. V. Bandura, J. Comput. Chem. **33**, 1123 (2012).
[53]R. D. Shannon, Acta Crystallogr. A **32**, 751 (1976).
[54]L. Liu, H. Guo, H. L, S. Dai, H. Cheng, and Z. Chena, J. Appl. Phys. **97**, 054102 (2005).
[55]Md. A. Mohiddon, P. Goel, K. L. Yadav, M. Kumar, and P. K. Yadav, Ind. J. Eng. Mater. Sci. **14**, 64 (2007).
[56]H. J. Hagemann, J. Phys. C: Solid State Phys. **11**, 3333 (1978).
[57]N.-H. Chan and D. M. Smyth, J. Am. Ceram. Soc. **67**, 285 (1984).
[58]H. M. Chan, M. P. Hamer, and D. M. Smyth, J. Am. Ceram. Soc. **96**, 507 (1986).
[59]J. Qi, Z. Gui, W. Li, Y. Wang, Y. Wu, and L. Li, Mater. Lett. **56**, 507 (2002).
[60]Y. Guang, W. Huan-Hua, T. Guo-Tai, J. An-Quan, Z. Yue-Liang, Y. Guo-Zhen, and C. Zheng-Hao, Chin. Phys. Lett. **18**, 1598 (2001).
[61]R. N. Schwartz, B. A. Wechsler, and L. West, Appl. Phys. Lett. **67**, 1352 (1995).
[62]V. Tura and L. Mitoseriu, Euro. Phys. Lett. **50**, 810 (2000).
[63]E. C. Subbarao and G. Shirane, J. Am. Ceram. Soc. **42**, 279 (1959).
[64]H. Yoo and C.-E. Lee, J. Am. Ceram. Soc. **88**, 617 (2005).
[65]M. C. Chang and S.-C. Yu, Adv. Quantum Chem. **37**, 179 (2000).
[66]J. Zhi, A. Chen, Y. Zhi, P. M. Vilarinho, and J. L. Baptista, J. Am. Ceram. Soc. **82**, 1345 (1999).
[67]T. Takeda and A. Watanabe, Jpn. J. Appl. Phys. **7**, 232 (1968).
[68]Y. Tsur, T. D. Dunbar, and C. A. Randall, J. Electroceram. **7**, 25 (2001).
[69]J. E. ten Elshof, H. J. M. Bouwmeester, and H. Verweij, Solid State Ionics **89**, 81 (1996).
[70]G. Y. Gou, J. W. Bennett, H. Takenaka, and A. M. Rappe, Phys. Rev. B **83**, 205115 (2011).
[71]J. W. Bennett, I. Grinberg, and A. M. Rappe, J. Am. Chem. Soc. **130**, 17409 (2008).
[72]M. Dawber and J. F. Scott, Appl. Phys. Lett. **76**, 1060 (2000).
[73]A. J. Moulson and J. M. Herbert, *Electroceramics: Materials, Properties and Applications* (Chapman and Hall, London, 1990).
[74]G. M. Keith, K. Sarma, N. M. N. Alford, and D. C. Sinclair, J. Electroceram. **13**, 305 (2004).
[75]F. D. Morrison, A. M. Coats, D. C. Sinclair, and A. R. West, J. Electroceram. **6**, 219 (2001).
[76]Y. Shuai, S. Zhou, D. Bürger, H. Reuther, I. Skorupa, V. John, M. Helm, and H. Schmidt, J. Appl. Phys. **109**, 084105 (2011).
[77]H. M. Al-Allak, J. Am. Ceram. Soc. **94**, 2757 (2011).
[78]S. Saha, T. P. Sinha, and A. Mookerjee, Phys. Rev. B **62**, 8828 (2000).